Supplementary Information for

Bioorthogonal Modification of the Major Sheath Protein of Bacteriophage M13: Extending the Versatility of Bionanomaterial Scaffolds

Taylor Urquhart, Elisabeth Daub and John Frank Honek*

Department of Chemistry and Waterloo Institute for Nanotechnology, University of Waterloo, 200 University Avenue, Waterloo, Ontario, Canada N2L 3G1

Methods and Materials

Construction of bacterial strains. An *E. coli* strain deficient in its methionine (**Met**) biosynthesis pathway and capable of infection by M13 was produced. *E. coli* K12 ER2738 (New England Biolabs, Whitby, ON, Canada) was the starting strain (F' *proA*$^{+}$*B*$^{+}$ *lacI*^{q} *Δ(lacZ)M15/ Δ(lac-proAB) glnV thi-1 Δ(hsdS-mcrB)5 FhuA2)*. This strain was mutated utilizing a $P1_{vir}$ transduction to inactivate two Met biosynthesis genes[1]. The two targeted genes were *metA* and *metE* which were inactivated using $P1_{vir}$ grown on JW3973-1 [Sex: F- Chromosomal markers: *Δ(araD-araB)567, ΔlacZ4787(::rrnB-3), λ*$^{-}$*, rph-1, ΔmetA780::kan, Δ(rhaD-rhaB)568, hsdR514*], or JW3805-1 [Sex: F- Chromosomal markers: *Δ(araD-araB)567, ΔlacZ4787(::rrnB-3), λ-, rph-1, ΔmetE774::kan, Δ(rhaD-rhaB)568, hsdR514*] as donor strains respectively[2]. Of these two mutations, only Δ*metE774::kan* resulted in complete dependence on an exogenous source of Met. The *metE* strain, referred to here as ER2738 *metE*, was used for *L*-azidohomoalanine (**Aha**) incorporation into M13.

Construction of M13 pVIII$_{M-5/28L}$ strain. The Met residues at positions -5 and 28 (mature pVIII numbering) of pVIII protein of WT M13 were mutated to leucine. M13KE (New England Biolabs, Whitby, ON, Canada) was the starting plasmid for these mutations. Site-directed mutagenesis of M-5L was carried out using the forward and reverse primers in **Supplementary Table 1**. The resulting plasmid M13KE-pVIII$_{M-5L}$ was transformed into *E. coli* K12 ER2738. Successful transformants were selected for by plaque formation on a lawn of *E. coli* K12 ER2738. M13KE M-5L plasmid DNA was then purified and subjected to site-directed mutagenesis using the primers for M28L. The resulting plasmid M13KE-pVIII$_{M-5/28L}$ was transformed into *E. coli* K12 ER2738 and selected for as above. Plaques were used to infect a 1:100 diluted overnight culture of *E. coli* K12 ER2738 for 4.5 hours at 37 ^{o}C. The cells were removed by centrifugation at 3200*g* for 5 minutes. The M13-containing supernatant was stored at -20 ^{o}C in 50% glycerol. The *E. coli* pellet was processed using the manufacturer's instructions for GeneJET Plasmid Miniprep kit (ThermoScientific, Ottawa, Canada). The success of mutations were confirmed by DNA sequencing.

Construction of single Met M13 variants. In order to explore the positioning of Met regarding Aha incorporation, single Met variants (pVIII$_{A9M}$, pVIII$_{S13M}$ and pVIII$_{A16M}$) were constructed. M13KE-pVIII$_{M-5/28L}$ constructed above was the starting point for the single Met variants. Site-directed mutagenesis was carried out using the forward and reverse primers as indicated in **Supplementary Table 1**. The mutant DNA was transformed into *E. coli* K12 ER2738. Successful transformants were selected for by plaque formation as above. The resulting plasmids are denoted M13KE-pVIII$_{A9M}$, M13KE-pVIII$_{S13M}$, and M13KE-pVIII$_{A16M}$ respectively. Plaques were used to infect an overnight culture of *E. coli* K12 ER2738

for 4.5 hours at 37 ^{o}C. The resulting M13 phage stocks were stored at -20 ^{o}C in 50% glycerol. Success of mutations were confirmed by DNA sequencing.

Supplementary Table 1: Primers used for site-directed mutagenesis of M13KE plasmid.

M-5L forward	5'-gttgctaccctcgttccgctgctgtctttcgctgctgag-3'
M-5L reverse	5'-ctcagcagcgaaagacagcagcggaacgagggtagcaac-3'
M28L forward	5'-atcggttatgcgtgggcgctggttgttgtcattgtcggc-3'
M28L reverse	5'-gccgacaatgacaacaaccagcgcccacgcataaccgat-3'
A9M forward	5'-ggtgacgatcccgcaaaaatggcctttaactccctgc-3'
A9M reverse	5'-gcagggagttaaaggccatttttgcgggatcgtcacc-3'
S13M forward	5'-gcaaaagcggcctttaacatgctgcaagcctcagcgacc-3'
S13M reverse	5'-ggtcgctgaggcttgcagcatgttaaaggccgcttttgc-3'
A16M forward	5'-ggcctttaactccctgcaaatgtcagcgaccgaatatatcgg-3'
A16M reverse	5'-ccgatatattcggtcgctgacatttgcagggagttaaaggcc-3'

Supplementary Table 2: Number of Met residues in proteins encoded by the M13 genome.

M13 protein	Number of Met*	Amino acids (% Met)
pI	3	348 (0.86)
pII	7	410 (1.71)
pro-pIII	8	424 (1.89)
pIII	7	406 (1.72)
pro-pIV	6	426 (1.41)
pIV	4	405 (0.99)
pV	2	87 (2.30)
pVI	1	112 (0.89)
pVII	2	33 (6.06)

pro-pVIII	3	73 (4.11)
pVIII	1	50 (2.0)
pIX	2	32 (6.25)
pX	3	111 (2.70)
pXI	1	108 (0.93)

*From genomic data[3]

General growth of M13 phages. Overnight cultures of *E. coli* strain ER2738 (New England Biolabs, Whitby, ON, Canada) were diluted 1:100 into 50 mL lysogeny broth (LB) media and infected with M13 at $1x10^6$ pfu/mL. Phage amplification was carried out at 37 ^oC for 4.5 hours. The culture was centrifuged at 12000*g* for 10 minutes to pellet *E. coli*. For comparing the amplification of M13 variants, the phage titres were determined by spotting-plating dilutions of the resulting supernatant onto lawns of *E. coli* ER2738. For testing the effect of media conditions on M13 production using *E. coli* ER2738 *metE* M9 minimal media (32 mM Na_2HPO_4, 22 mM KH_2PO_4, 61 mM NaCl, 76 mM $(NH_4)_2SO_4$, 1 mM $MgSO_4$, 0.1 mM $CaCl_2$, 0.1% thiamine·HCl, 11 mM D-glucose, pH 7.4) was used instead of LB media with the following supplementations (μg/mL): Phe (50), Lys (50), Arg (125), Gly (10), Val (35), Ala (42), Trp (20), Thr (35), Ser (420), Pro (230), Asn (48), Asp (52), Gln (730), Glu (935), Tyr (18), Ile (40), Leu (40), His (50) and Cys (50). The amount of Met was varied as indicated.

Aha incorporation into M13. The method used to incorporate Aha (Bachem, Bubendorf, Switzerland) into M13 was adapted from that used by van Hest *et al.* for a single overexpressed protein[4]. An overnight culture of *E. coli* strain ER2738 *metE* (Supplementary Methods) was diluted 1:100 into 50 mL of LB media and grown to an A_{600} of 1.0. Cells were pelleted at 12000*g* for 5 minutes, washed with M9 minimal media, pelleted at 12000*g* for 5 minutes and resuspended in M9 minimal media supplemented with amino acids as described above and either 0 or 10 mM Aha added. In addition, Met was added to a final concentration of 235 μM. At this point, the culture was infected with $M13_{WT}$ or M13 variant (Supplementary Methods and Supplementary Table 1) to a titre of $1x10^6$ pfu/mL. M13 was grown for 4.5 hours at 37 ^oC. The culture was centrifuged at 12000*g* for 10 minutes to pellet *E. coli* and the supernatant was retained.

The supernatant was mixed with a 1/5 volume of 20% PEG-8000/1M NaCl and incubated for 18 hours at 4 ^oC. The resulting mixture was centrifuged at 12000*g* for 15 minutes. The pellet was resuspended in 2 mL of PBS buffer and 0.4 mL of 20% PEG-8000/1M NaCl and incubated for 30 min. A

microcentrifuge was used to pellet the precipitated phages (15000*g* for 10 minutes). The resulting pellet was resuspended in 0.4 mL of 1x PBS buffer (10 mM Na_2HPO_4, 1.8 mM KH_2PO_4, 137 mM NaCl, 2.7 mM KCl, pH 7.4). The solution was spun once more at 15000*g* for 1 min to clear the supernatant which was retained, and a phage titre was determined.

Strain-promoted azide-alkyne cycloaddition of Aha-pVIII. M13 phages ($1x10^{13}$ pfu/mL) were reacted with either 30 μM DIBAC-PEG_4-TAMRA (Click Chemistry Tools, Scottsdale, AZ, USA) or 30 μM DIBAC-PEG_4-biotin (Click Chemistry Tools, Scottsdale, AZ, USA) labels in 1x PBS pH 7.8 for 24 hours at 23 °C. Excess label was removed by spin filtration using a Pall Nanosep® 10 kDa MWCO column (Sigma-Aldrich, Milwaukee, WI, USA) and washed at least three times with 0.5 mL of 1x PBS. Absorbance spectra of TAMRA-labeled M13 were read on a SpectraMax M5 (Molecular Devices, Sunnyvale, CA, USA) scanning from 240-650 nm. Dual-labeled M13 conjugates were prepared as above with the exception of adding 100 μM NHS-sulfo-cy7 (Lumiprobe Corporation, Hallandale Beach, Florida, USA) and 100 μM DIBAC-TAMRA or DIBAC-biotin at 4 °C for 24 hours.

Calculating labeling efficiency. The phage titres were estimated from absorbance using equation (1) where N_{bp} is the number of base pairs in the phage genome[5]. The $6x10^{16}$ coefficient can be derived from the extinction coefficient of 3.84 $mg^{-1}cm^{-1}mL$[6]. Note, this equation has been modified to include a correction factor (CF) which accounts for absorbance at 269 nm from TAMRA. The CF was estimated to be 0.65 from a spectrum of 5 μM DIBAC-PEG_4-TAMRA in 1x PBS. From the titre, the number of pVIII subunits was estimated by approximating 2700 pVIII subunits per M13 in equation (2). The labeling efficiency was then estimated using equation (3) where ε_{dye} equal to 65000 M^{-1} cm^{-1} was the extinction coefficient for TAMRA[7] and subtracting A_{590} in order to correct for non-specific absorbance.

$$[M13] = \frac{(A_{269} - A_{556} \times CF - A_{320}) \times 6 \times 10^{16}}{N_{bp}} \quad (1)$$

$$[pVIII] = [M13] \times \frac{2700\ pVIII}{M13} \times \frac{1000\ mL}{L} \times \frac{1\ mol\ M13}{6.02 \times 10^{23}\ M13} \quad (2)$$

$$\%eff. = \frac{(A_{556} - A_{590})}{\varepsilon_{dye} \times [pVIII]} \times 100\% \quad (3)$$

Mass spectrometry of M13. M13 samples were exchanged into Milli-Q water (MQH_2O; ultra-pure 18 MΩ·cm resistivity; Millipore, Canada) using a Pall Nanosep® 10 kDa MWCO column. Samples were analyzed using a Micromass Q-TOF Ultima Global (Waters, Milford, Mass., USA) equipped with a nano ESI source or a Thermo Scientific Q-Exactive Orbitrap equipped with an ESI source. Mass spectra

collected on the Micromass Q-TOF were from samples run in 1:1 H_2O:MeCN 0.2% formic acid. Mass spectra collected on the Q-Exactive were from samples run in 1:1 H_2O:MeOH 0.1% formic acid.

Transmission electron microscopy. Sample grid preparation was adapted from Ploss, M. and Kuhn, A.[8]. M13 samples at 10^{10} pfu/mL in MQH_2O were deposited onto a carbon-formvar coated 400 mesh grid (Canemco-Marivac, Gore, QC, Canada) for 1 min followed by 0.1% bovine serum albumin (BSA) in tris-buffered saline (50 mM tris(hydroxymethyl)aminomethane, 150 mM NaCl, pH 7.5) for 10 min. Excess BSA was blotted off and the grid was exposed to 20 µL of a 1:10 dilution of 0.15 mg/mL SA-AuNP solution (Cytodiagnostics, Burlington, Ontario, Canada) for 30 min at 23 ^oC. After two washes with MQH_2O, the grid was stained for two minutes using 1% uranyl acetate. M13 phages were imaged at 60 kV using a CM10 Philips microscope modified with an Advanced Microscopy Techniques image capturing CCD camera.

Streptavidin-conjugated magnetic particles assay and immuno-detection. M13 conjugates were incubated with 5 mg/mL 1 µm diameter SA-conjugated magnetic particles (New England Biolabs, Whitby, ON, Canada) for 30 min at 23 ^oC in 1x PBS pH 7.8. The SA-conjugated magnetic particles were removed by application of a magnet for 2 min. The supernatant was recovered and analysed by absorbance spectroscopy. Extent of binding of M13 to the particles was determined by quantifying the amount of M13 in the supernatant before and after incubation[9]. M13 was quantified by its absorbance at 269 nm as described above.

Binding of M13 to SA-conjugated magnetic particles was further confirmed utilizing anti-pVIII antibodies to detect bound M13. This served to validate the assumption that the decrease of M13 absorbance could be attributed to M13 binding to the SA-conjugated magnetic particles. Magnetic particles with bound phage or control were "blocked" with 3% bovine serum albumin (BSA) in 1x PBS pH 7.8 for 1 hour at 23 ^oC. The magnetic particles were separated with application of a magnet for 2 min and washed with 1x PBS pH 7.8 with 0.05 % Tween-20 (PBST). This was repeated for a total of three washes. Next, anti-pVIII mouse IgG antibodies (Santa Cruz Biotechnology, Inc., Dallas, Texas, USA) at 1 µg/mL in PBST was added for 1 hour at 23 ^oC. The magnetic particles were separated and washed three times with PBST as described above. Next, anti-mouse goat IgG antibodies conjugated to horseradish peroxidase (HRP) (Santa Cruz Biotechnology, Inc., Dallas, Texas, USA) at 0.8 µg/mL in PBST was added for 1 hour at 23 ^oC. The magnetic particles were separated and washed five times with PBST as described above. The final wash was done in 0.1 M citrate pH 6.0. HRP detection was carried out using 3,3′,5,5′-tetramethylbenzidine (TMB) as described previously[10]. The detection solution was prepared by mixing 100 µL of 10 mg/mL TMB in DMSO with 9.9 mL of 0.1 M citrate pH 6.0 with 1.3 mM H_2O_2. To

detect HRP, 150 µL of this solution was added to magnetic particles. After 1.5 min, 50 µL of 1 M H_2SO_4 was added and the absorbance at 450 nm was read.

Supplementary Results

Growth of M13-Aha constructs. Amplification of M13 was carried out using different growth conditions and a methionine auxotrophic *E. coli* to encourage Aha incorporation into M13 coat proteins. For example, when infecting *E. coli* ER2738 *metE* with M13, no amplification was observed at concentrations of Met at or below 34 µM (**Supplementary Figure 1b,c**). In the absence of Met, a high concentration of Aha (2 mM) alone was not sufficient for amplification of M13 either (**Supplementary Figure 1b**). Phage amplification with 10 mM Aha in the presence of Met (235 µM) resulted in a 3.4-fold, 2-fold and 4.4-fold decrease in yield for $M13_{A9M}$, $M13_{S13M}$ and $M13_{A16M}$ phages respectively compared to conditions lacking Aha (**Supplementary Figure 1d**). Interestingly, even for the Met-less variant, $M13_{M\text{-}5/28L}$, growth in the presence of Aha also resulted in a decrease in phage production (**Supplementary Figure 1d**). The lower yields obtained for $M13_{M\text{-}5/28L}$ produced with Aha suggest that the loss in viability is not due to destabilization of pVIII. The M13 life cycle requires that multiple proteins be co-expressed and be able to self-assemble at the pI/pIV/pXI complex at the *E. coli* cell membrane[11]. These may be affected by Aha substitution. Importantly, it was found here that having a defined concentration of Met in the growth medium would allow for successful and appreciable titre of M13 to be reached in the presence of Aha.

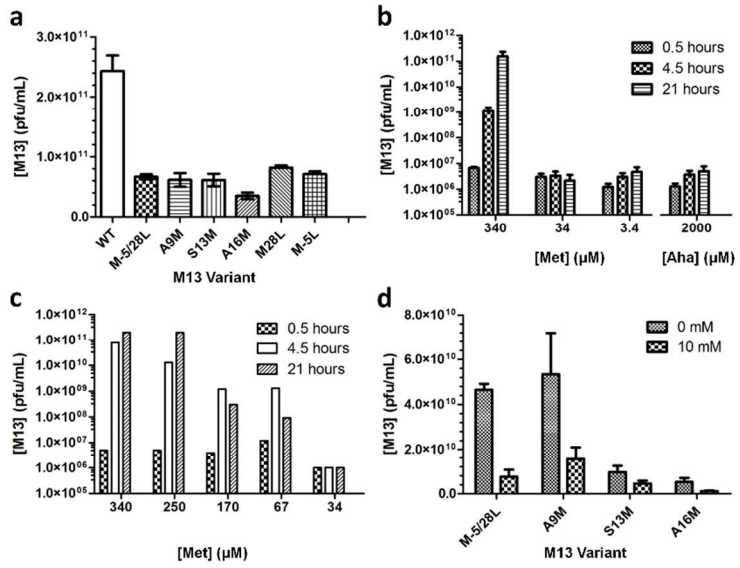

Supplementary Figure 1: Growth properties of M13 phages. (a) Comparison of viabilities of the various M13 variants at 4.5 hour amplification time using ER2738 *metE E. coli* as host in LB media. *E. coli* cells were infected at a starting phage titre of 10^6 pfu/mL. The A9M, S13M and A16M variants also contained both the M-5/L and M28L mutations. (b, c) $M13_{A9M}$

production using the Met auxotrophic host as outlined in Methods employing M9 minimal media with defined concentrations of Met or Aha as shown. Aha experiments in (b) were done in the absence of Met. Aliquots from the growth medium were titred at the indicated times. Results for an extended range of Met concentrations (34-340 µM) is provided in (c). (d) Comparison of viabilities of the various M13 variants at 4.5 hour amplification time using ER2738 metE *E. coli* as host and M9 minimal media with 235 µM Met and either 0 or 10 mM Aha. Cells were infected at a starting titre of 10^6 pfu/mL. (a, b, d are n=3 and c is n=1).

Mass spectrometry of M13-Aha constructs. In order to assess the incorporation of Aha into pVIII, electrospray ionization mass spectrometry (**ESI-MS**) was employed. In the main text, a percentage of $pVIII_{A9M}$ contained Aha residues in place of Met (**Figure 2**). This analysis was extended to S13M, Wt and M-5/28L pVIII variants as well. With the exception of $pVIII_{M\text{-}5/28L}$ peaks associated with pVIII containing Met and pVIII containing Aha were detected in the mass spectrum of each variant of M13.

The expected mass of the variant $pVIII_{A9M}$ was 5280.1 Da. The primary peak was observed at 5279 Da and likely corresponded to pVIII with Met incorporated (pVIII-Met). In the spectrum of $pVIII_{A9M}$ grown in the presence of 10 mM Aha, in addition to the primary peak at 5279 Da, a peak at 5274 Da was also observed (**Supplementary Figure 2**). The intensity of the secondary peak was 10.2 % of the primary peak. This secondary peak indicated that a portion of total pVIII subunits had Aha incorporated in place of Met.

For the variant $pVIII_{S13M}$, the expected mass of the construct was 5264.1 Da. The primary peak in the mass spectrum of $pVIII_{S13M}$ grown in the absence of Aha was at 5263 Da and corresponded well with the expected mass of $pVIII_{S13M}$ (**Supplementary Figure 3**). In the spectrum of $pVIII_{S13M}$ grown in the presence of 10 mM Aha a secondary peak was also observed at 5258.5 Da and likely corresponded to $pVIII_{S13M}$ with Aha having replaced Met13. The intensity of the secondary peak was 13.4 % of the primary peak. This indicated that a portion of total pVIII subunits had Aha incorporated in place of Met.

For WT pVIII, the expected mass was 5238 Da. The primary peak in the mass spectrum of WT pVIII grown in the absence of Aha was observed at 5236.5 Da and corresponded well with the expected mass of WT pVIII (**Supplementary Figure 4**). In the spectrum of WT pVIII grown in the presence of 10 mM Aha, a secondary peak was also observed at 5232.5 Da and likely corresponded to pVIII with Aha having replaced Met28. The intensity of the secondary peak was 11.3 % of the primary peak. For WT M13, this indicated that a portion of total pVIII subunits had Aha incorporated in place of Met. Overall, there was a similarity in the ratio of pVIII-Aha to pVIII-Met peak signal intensities in the mass spectra between A9M, S13M and Wt M13. Since these proteins only differed by minor point mutations, the levels of Aha incorporation were consistent between A9M, S13M and Wt pVIII M13 strains.

In the control strain, $pVIII_{M\text{-}5/28L}$, the mass spectra of samples produced in the presence or absence of Aha were very similar. The expected mass of $pVIII_{M\text{-}5/28L}$ was 5220 Da. The primary peak in the mass

spectrum of $pVIII_{M\text{-}5/28L}$ grown in the absence of Aha was observed at 5218.5 Da and corresponded well with the expected mass of $pVIII_{M\text{-}5/28L}$ (**Supplementary Figure 5**). In the spectrum of $pVIII_{M\text{-}5/28L}$ grown in the presence of 10 mM Aha, no secondary peak was observed that might correspond to $pVIII_{M\text{-}5/28L}$ with Aha incorporated. This suggested there was no incorporation of Aha in this case, which was expected given the lack of Met residues in the sequence of $pVIII_{M\text{-}5/28L}$. This control indicated that incorporation of Aha was specific to the replacement of Met only, which was consistent with previous studies on Aha incorporation into proteins.

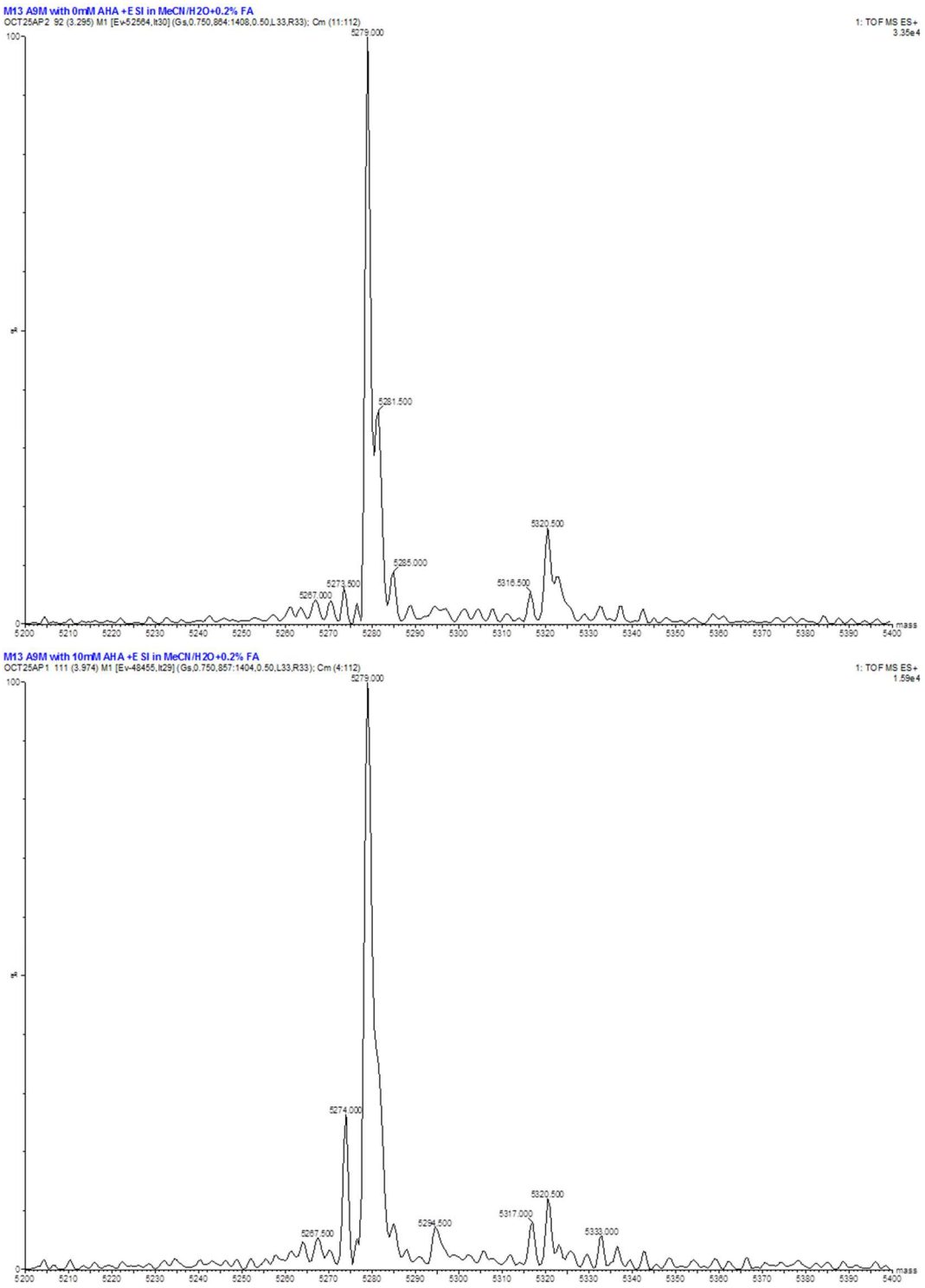

Supplementary Figure 2: Deconvoluted ESI-TOF mass spectra of $M13_{A9M}$ grown without (top) and with 10 mM Aha (bottom) in the presence of 235 µM Met. These samples were analyzed on a Waters Q-TOF instrument and deconvoluted using MassLynx™ 4.0 Global software with a resolution of 0.5 Da.

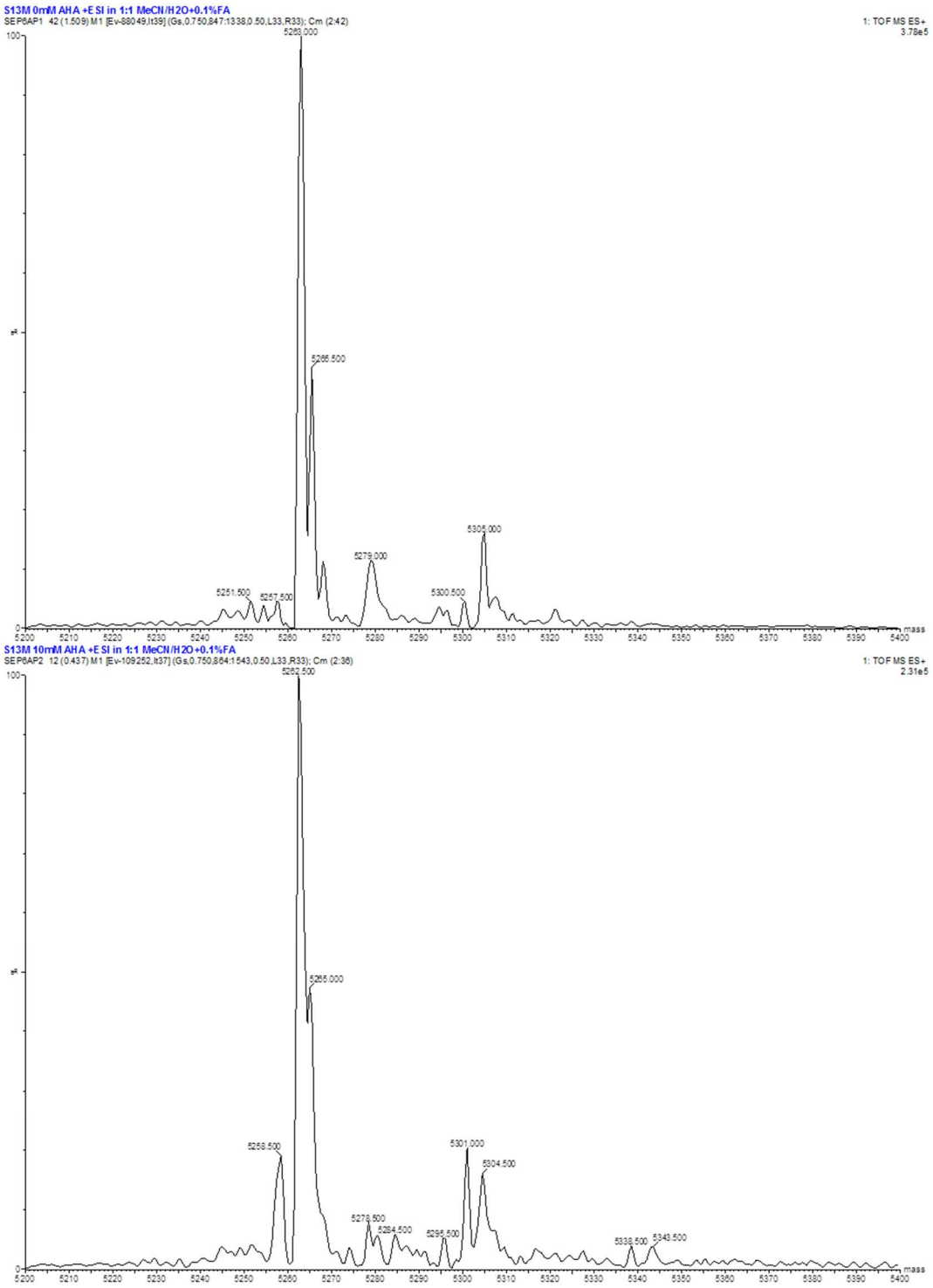

Supplementary Figure 3: Deconvoluted ESI-TOF mass spectra of M13$_{S13M}$ grown in the presence of 235 µM Met without (top) and with 10 mM Aha (bottom). These samples were analyzed on a Waters Q-TOF instrument and deconvoluted using MassLynx™ 4.0 Global software with a resolution of 0.5 Da.

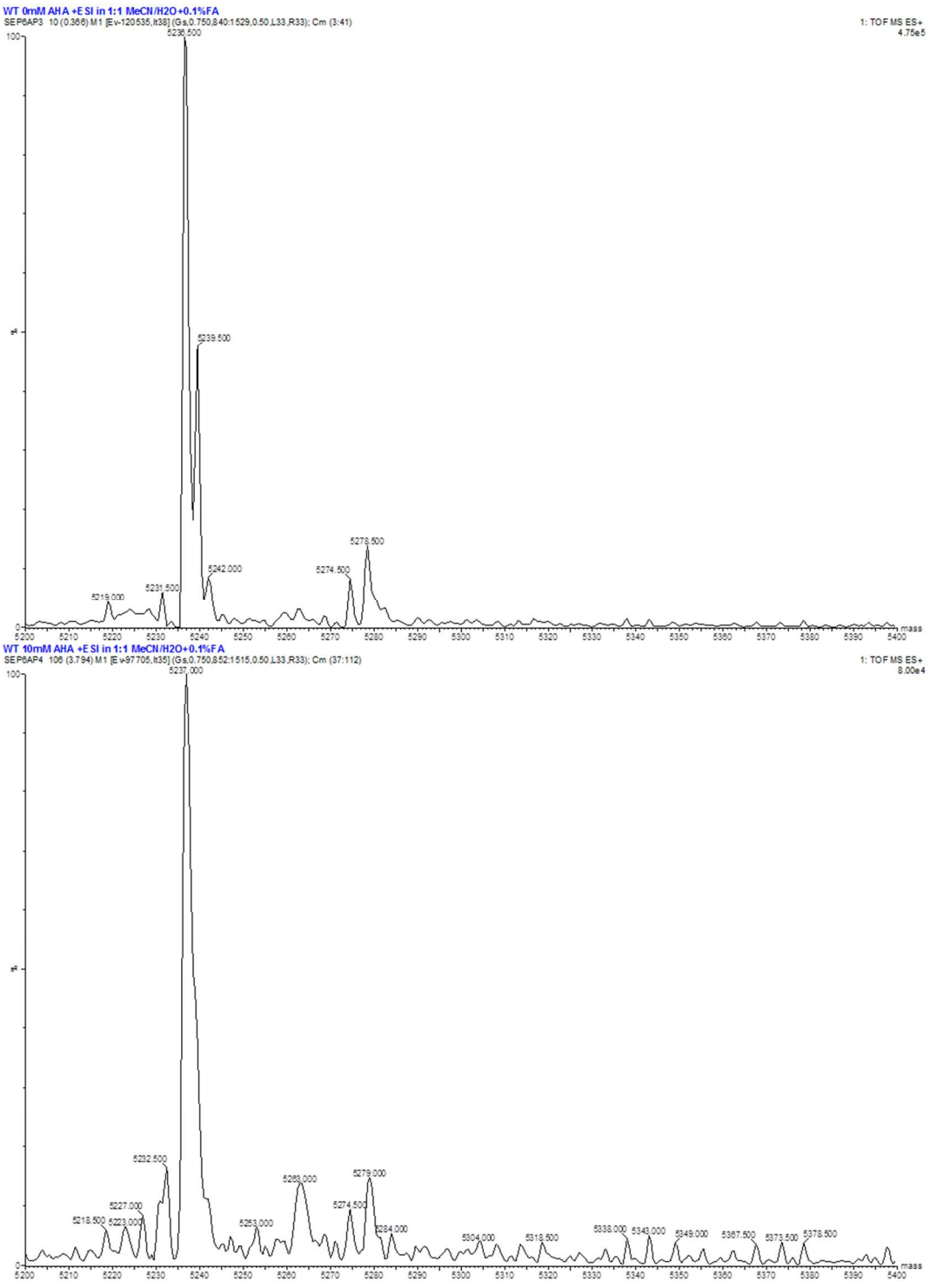

Supplementary Figure 4: Deconvoluted ESI-TOF mass spectra of M13$_{WT}$ grown in the presence of 235 µM Met without (top) and with 10 mM Aha (bottom). These samples were analyzed on a Waters Q-TOF instrument and deconvoluted using MassLynx™ 4.0 Global software with a resolution of 0.5 Da.

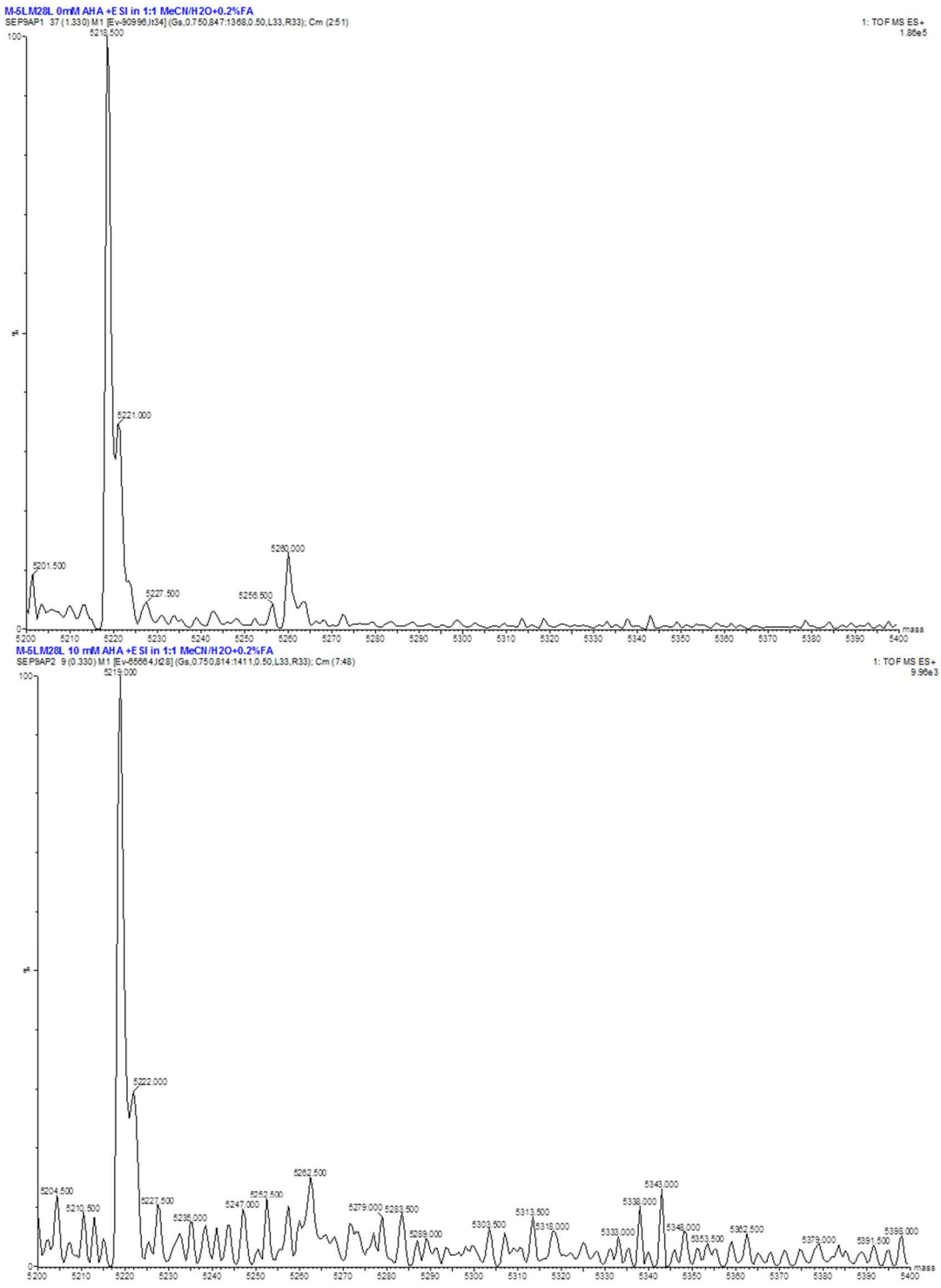

Supplementary Figure 5: Deconvoluted ESI-TOF mass spectra of $M13_{M\text{-}5/28L}$ grown in the presence of 235 µM Met without (top) and with 10 mM Aha (bottom). These samples were analyzed on a Waters Q-TOF instrument and deconvoluted using MassLynx™ 4.0 Global software with a resolution of 0.5 Da.

Transmission electron microscopy of M13 constructs visualized with gold-nanoparticles. In the main text, the loading of streptavidin-labeled gold nanoparticles (**SA-AuNPs**) onto assembled M13 phages was examined. Briefly, M13 samples were reacted via the strain-promoted azide-alkyne cycloaddition (**SPAAC**) reaction with DIBAC-biotin and visualized with SA-AuNPs. It was found that reaction via the SPAAC reaction and subsequent loading SA-AuNPs was successful with $pVIII_{A9M}$ and $pVIII_{S13M}$ but not with Wt pVIII. The incorporation of Aha into variant M13 $pVIII_{S13M}$ was visualized by transmission electron microscopy (**TEM**) as described in the main methods (**Figure 4**).

M13 $pVIII_{A9M}$ grown in the absence of Aha did not template the binding of AuNPs after reaction with DIBAC-biotin (**Supplementary Figure 6A**). The few SA-AuNPs that could be seen bound to each M13 particle were likely through non-specific interactions. M13 $pVIII_{A9M}$ samples grown in the presence of Aha were able to template the binding of 53-54 AuNPs on average (**Supplementary Figure 6B**). This was similar to the loading seen for the variant $pVIII_{S13M}$ (**Supplementary Figure 7**). As with the M13 $pVIII_{S13M}$ variant, M13 $pVIII_{A9M}$ also appeared to be a suitable mutation for producing an M13 scaffold capable of loading large particles.

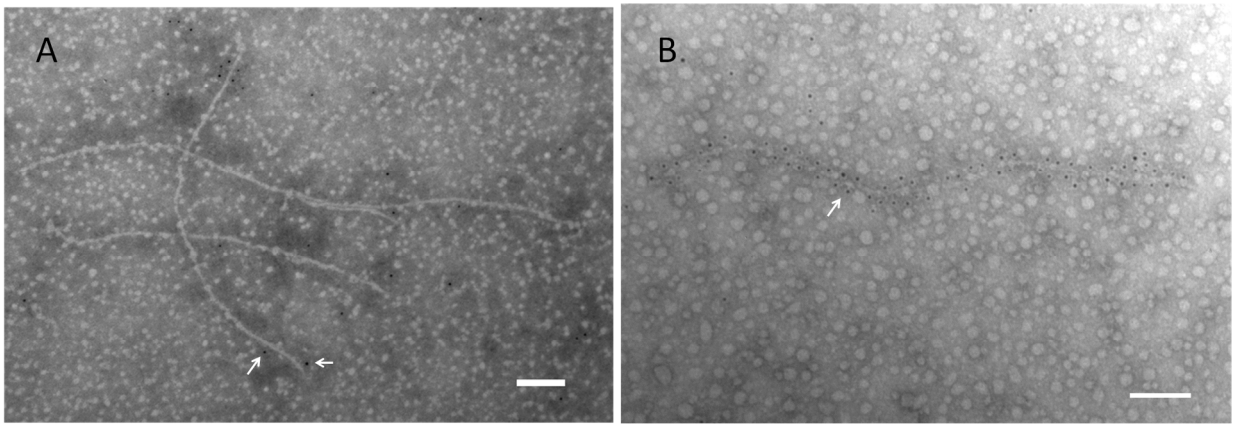

Supplementary Figure 6: TEM image of $M13_{A9M}$ constructs visualized with 5 nm SA-AuNPs. (A) $M13_{A9M}$ grown in the presence of 235 µM Met but in the absence of Aha and reacted with DIBAC-PEG_4-biotin. (B) $M13_{A9M}$ grown with 10 mM Aha and reacted with DIBAC-PEG_4-biotin. White arrows show AuNPs and the white scale bar shows 100 nm.

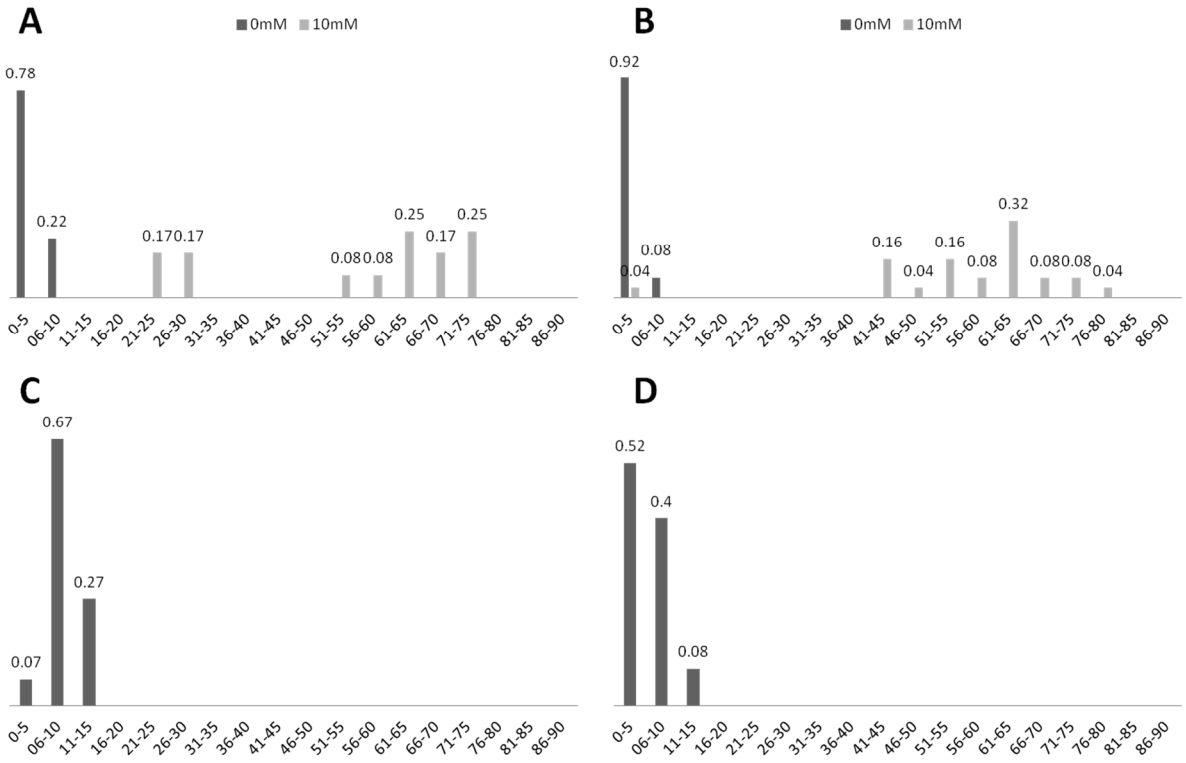

Supplementary Figure 7: Histogram of frequencies of SA-AuNPs bound to M13 constructs after reacting with DBCO-PEG$_4$-biotin observed on TEM images. (A) M13$_{A9M}$ grown in the presence of 235 µM Met but in the absence or presence of 10 mM Aha (0 mM Aha: n=9, 10 mM Aha: n=14). (B) M13$_{S13M}$ grown in the presence of 235 µM Met and in the absence or presence of 10 mM Aha (0 mM Aha: n=24, 10 mM Aha: n=25). (C) M13$_{WT}$ grown with 10 mM Aha (n=15). (D) M13$_{M-5/28L}$ grown with 10 mM Aha (n=50).

WT M13 that had been prepared in the presence of Aha was conjugated with biotin and labeled with SA-AuNPs. The average number of SA-AuNPs seen associated with each M13 particle was lower than that seen for A9M or S13M at 8 AuNPs per phage (**Figure 4d**). In addition to lower AuNP binding, changes to the usual M13 morphology were observed. The TEM micrographs showed WT M13 phages with sharp bends rather than with normal linearity (**Supplementary Figure 8**). The low binding of SA-AuNPs was likely due to the predicted low solvent accessibility of the Met28 residue position. DIBAC-biotin reacted with Aha incorporated at Met28 could interfere with the usual packing of pVIII subunits of M13. This might have led to the perturbations in M13 structures seen here.

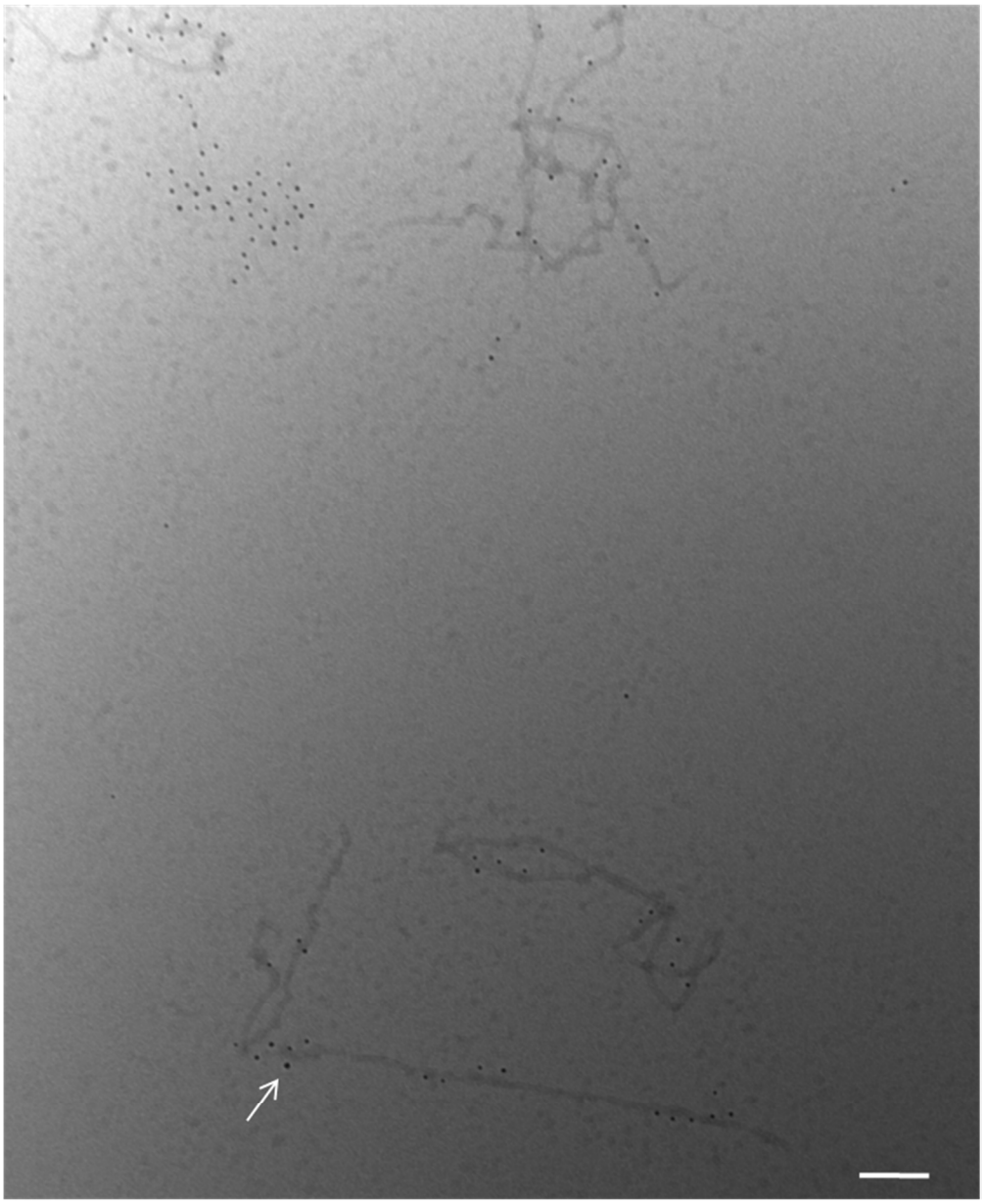

Supplementary Figure 8: TEM image of $M13_{WT}$ constructs visualized with 5 nm SA-AuNPs. $M13_{WT}$ was grown in the presence of 235 µM Met and with 10 mM Aha and reacted with DIBAC-PEG_4-biotin. White arrows show AuNPs and the white scale bar shows 100 nm.

M13 $pVIII_{M\text{-}5/28L}$ was used as a control for the TEM experiments since it was shown not to incorporate Aha. Samples of this variant were prepared in 10 mM Aha/235 µM Met and reacted with DIBAC-biotin as described in the main methods. Visualization with TEM showed minimal binding of SA-AuNPs to this variant after reaction with DIBAC-biotin (**Supplementary Figure 9**). Given the specificity of the DIBAC-biotin reagent for an azide functional group, it was expected that low AuNP particle binding would be seen. On average there was considerably more SA-AuNPs seen associated with

A9M and S13M M13 phages prepared with Aha on TEM than either the M-5/28L control or Wt strains (**Supplementary Figure 7**). Analysis of this control suggested that the binding of SA-AuNPs to A9M and S13M M13 variants was due to specific reaction of DIBAC-biotin to incorporated Aha residues. In combination with the TEM results of the A9M and S13M M13 variants, the loading of particles onto an M13 scaffold can indeed be achieved with high specificity using the incorporated azide specifically. In this control sample, some of the phages counted had a SA-AuNP associated near the tips of the particle. Given the sequences of the tip proteins pIII, pVI, pVII and pIX, and five copies of each in assembled M13, a maximum of 60 Met residues in each assembled M13 are present in the minor coat proteins (**Supplementary Table 2**). From crystallography of the two N-terminal domains, it is likely that Met135 of pIII is accessible and Met176 of pIII is buried[12]. The other 5 Met residues of pIII are on the C-terminal domain, although their solvent accessibility is unknown due to the lack of structural information for this section of the pIII protein. A more conservative estimate of the number of solvent-exposed Met residues on the minor coat proteins is 55 Met residues maximum, although in reality a reduced number are likely capable of reaction. Compared to approximately 2700 pVIII copies per M13, only 2% of the Met residues come from the minor coat proteins. It is therefore expected that the majority of Aha incorporation occurs on pVIII coat proteins, leaving the pIII coat proteins largely available to display peptides identified by standard phage display approaches.

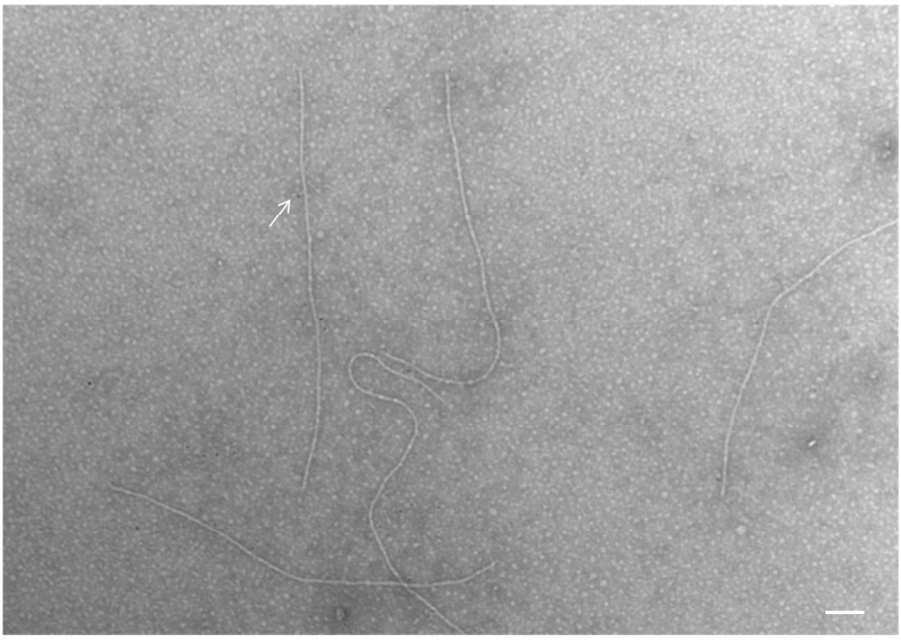

Supplementary Figure 9: TEM image of $M13_{M\text{-}5/28L}$ constructs visualized with 5 nm SA-AuNPs. $M13_{M\text{-}5/28L}$ was grown with 10 mM Aha/235 µM Met and reacted with DIBAC-PEG_4-biotin. White arrows show AuNPs and the white scale bar shows 100 nm.

Mass spectra of M13-Aha constructs post-reaction with DIBAC-biotin. M13 variants that were prepared with Aha and reacted with DIBAC-biotin for TEM analysis were also analysed by ESI-MS. For $pVIII_{A9M}$-Aha samples, reaction with DIBAC-biotin yielded a mass peak with the expected product of the SPAAC reaction at 6021 Da (**Supplementary Figure 10**). The primary peak at 5276.8 Da in this spectrum was consistent with the monoisotopic mass expected for $pVIII_{A9M}$. The peak associated with $pVIII_{A9M}$-Aha at -5 Da to the primary peak was not detected in this spectrum. The absence of the $pVIII_{A9M}$-Aha peak further supported successful reaction with DIBAC-biotin.

For $pVIII_{S13M}$-Aha samples, reaction with DIBAC-biotin yielded a mass peak with the expected product of the SPAAC reaction at 6005 Da (**Supplementary Figure 11**). The primary peak at 5260.8 Da in this spectrum was consistent with the monoisotopic mass expected for $pVIII_{S13M}$. As with $pVIII_{A9M}$, the peak associated with $pVIII_{S13M}$ containing Aha was not detected, and this was likely due to its reaction with DIBAC-biotin.

For WT pVIII-Aha samples, reaction with DIBAC-biotin did not yield a mass peak for the expected product of this reaction (**Supplementary Figure 12**). This was predicted to appear at 5980 Da. The primary peak at 5234.7 Da in this spectrum was consistent with the monoisotopic mass expected for WT pVIII. Also, WT pVIII which contained Aha was detected in this spectrum at 5229.7 Da and further suggested that WT pVIII did not successfully react with DIBAC-biotin. It is possible that if there were any WT pVIII-biotin conjugates, they were below detection limits of the instrument. This was also consistent with what was observed in TEM micrographs of WT M13 that had been reacted with DIBAC-biotin which showed minimal binding of SA-AuNPs. The TEM micrographs are also consistent with the conclusion that WT pVIII-Aha reacted poorly with the DIBAC-biotin reagent.

For $pVIII_{M\text{-}5/28L}$-Aha samples, reaction with DIBAC-biotin did not yield a peak that might indicate reaction with DIBAC-biotin (**Supplementary Figure 13**). It was expected that no conjugation would occur since no Met residues were present on mature $pVIII_{M\text{-}5/28L}$ for Aha incorporation. The primary peak at 5216.7 Da in this spectrum was consistent with the monoisotopic mass expected for $pVIII_{M\text{-}5/28L}$. This control spectrum makes it more reasonable to suggest that the SPAAC reaction proceeded as expected and was specific for incorporated Aha. Only for the two engineered M13 variants, A9M and S13M, was this reaction successful. It was likely that better solvent accessibility of Aha at A9 or S13 were the reason for the better reactivity compared to WT pVIII. The ESI-MS results here also closely match what was expected from the TEM analysis of M13 variants with conjugated biotin and show that biotin was covalently attached to pVIII subunits via the SPAAC linkage formed.

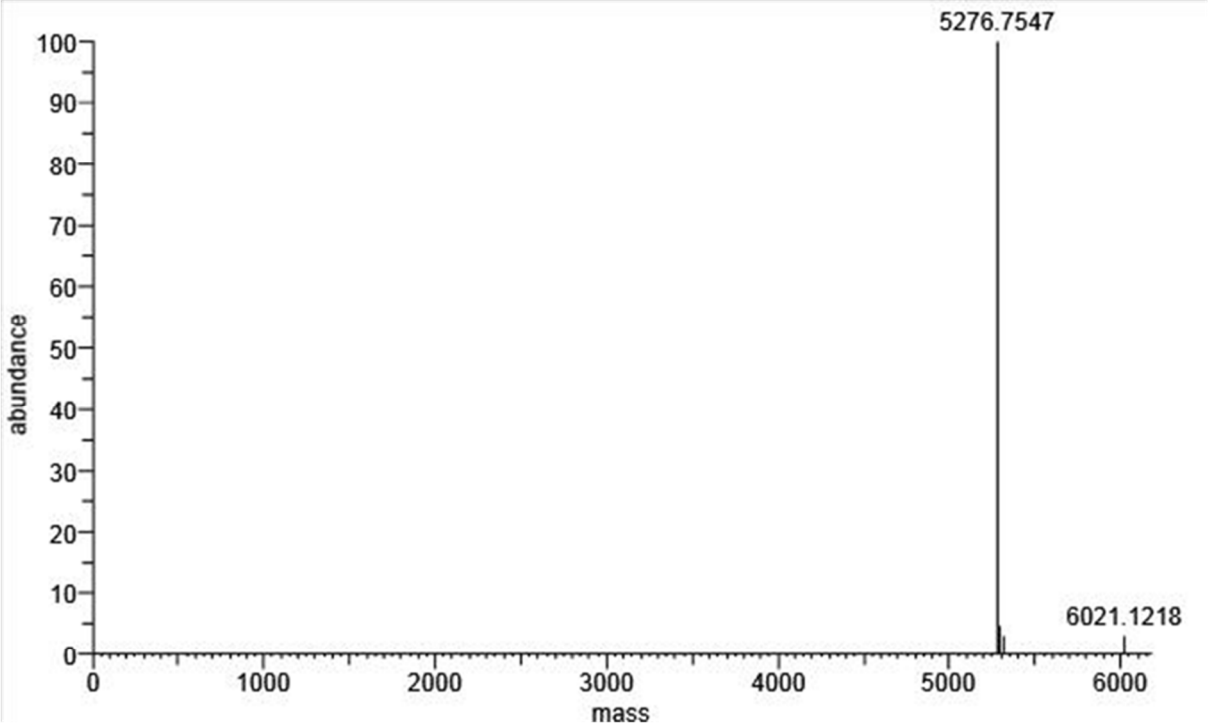

Xtract Masses Table				
Monoisotopic Mass	Sum Intensity	Number of Charge State	Average Charge	Delta Mass
5276.755	3149007	4	5.16	0
5292.769	151252.6	2	5.44	16.0145
6021.122	98396.78	2	5.57	744.3671
5317.731	95047.35	1	5	40.9761

Supplementary Figure 10: Deconvoluted mass spectrum of $M13_{A9M}$ grown with 10 mM Aha/235 µM Met and reacted with 30 µM DBCO-PEG_4-biotin via the SPAAC reaction. This spectrum was obtained utilizing a Fisher Scientific ESI-orbitrap instrument.

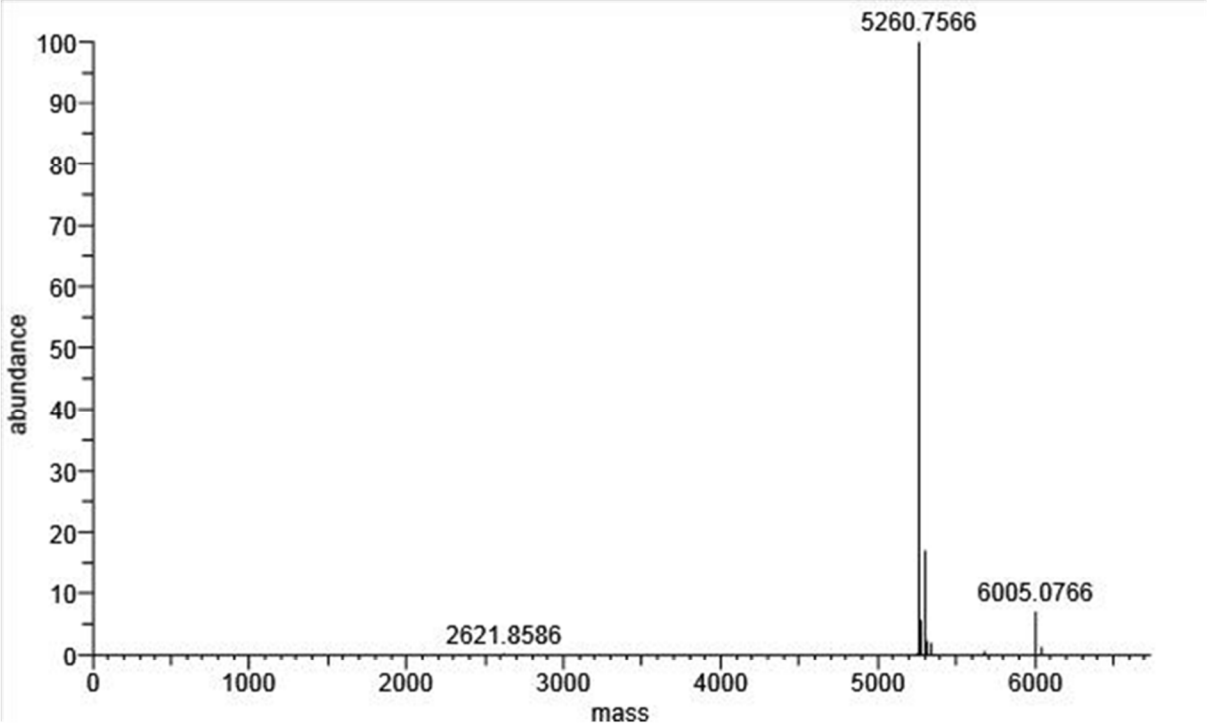

Xtract Masses Table				
Monoisotopic Mass	Sum Intensity	Number of Charge State	Average Charge	Delta Mass
5260.757	392651.7	5	5.5	0
5298.687	66872.06	5	5.88	37.93
5302.737	34293.72	4	5.19	41.9808
6005.077	28467.27	3	5.96	744.32
5276.725	22778.67	3	5.76	15.9684
5314.661	9226.71	3	5.89	53.9041
5340.662	8095.19	2	5.52	79.9051
5282.713	7219.71	3	5.99	21.9559
6043.064	5354.79	2	6.39	782.3075
5674.941	3279.11	1	6	414.1848
5245.722	2548.4	1	5	-15.0348
2621.859	2106.77	1	3	-2638.9
5336.663	1287.01	1	6	75.9063

Supplementary Figure 11: Deconvoluted mass spectrum of $M13_{S13M}$ grown with 10 mM Aha/235 µM Met and reacted with 30 µM DBCO-PEG_4-biotin via the SPAAC reaction. This spectrum was obtained utilizing a Fisher Scientific ESI-orbitrap instrument.

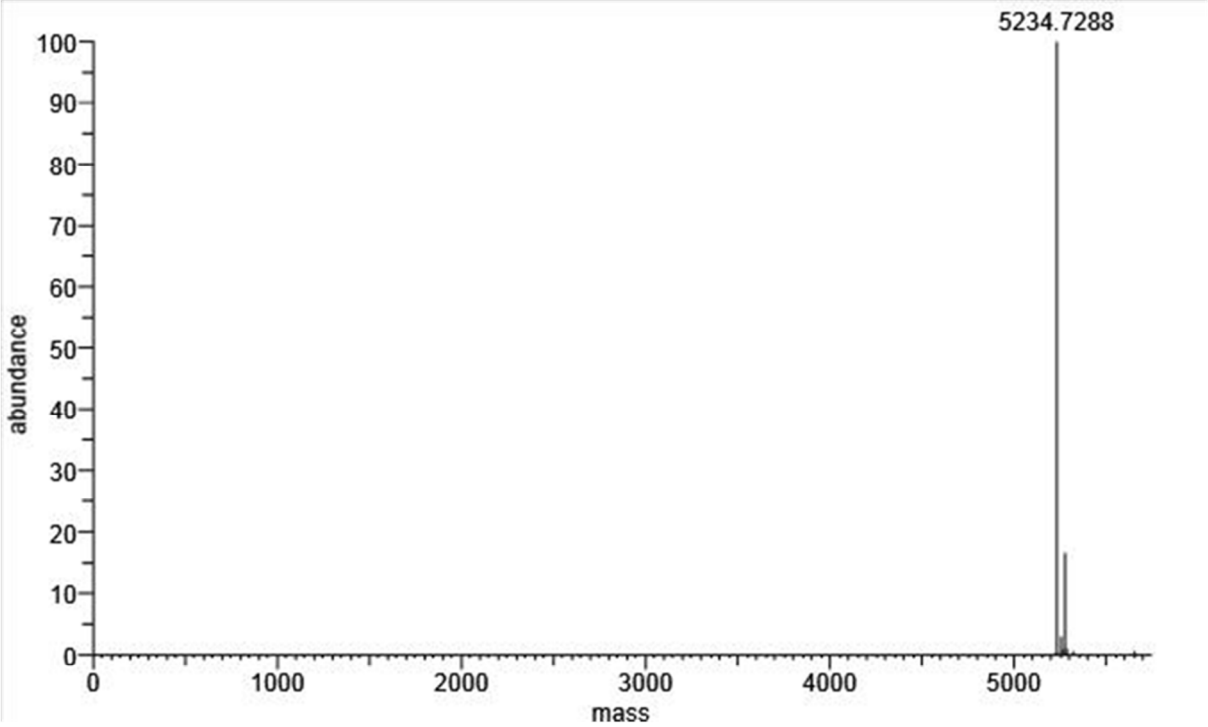

Xtract Masses Table				
Monoisotopic Mass	Sum Intensity	Number of Charge State	Average Charge	Delta Mass
5234.729	2709839	4	5.38	0
5272.674	452520.7	4	5.9	37.9451
5229.722	213084.8	3	5.59	-5.0069
5276.71	94007.57	2	5.24	41.9807
5250.735	88728.52	3	5.89	16.0066
5287.656	29179.62	2	6.35	52.9271
5267.69	29057.72	2	5.78	32.9611
5648.913	19681.5	1	6	414.1844
5314.658	19608.38	1	6	79.9287
5219.732	11151.09	1	5	-14.9968
5235.733	8635.51	1	8	1.0042

Supplementary Figure 12: Deconvoluted mass spectrum of $M13_{WT}$ grown with 10 mM Aha/235 µM Met and reacted with 30 µM DBCO-PEG_4-biotin via the SPAAC reaction. This spectrum was obtained utilizing a Fisher Scientific ESI-orbitrap instrument.

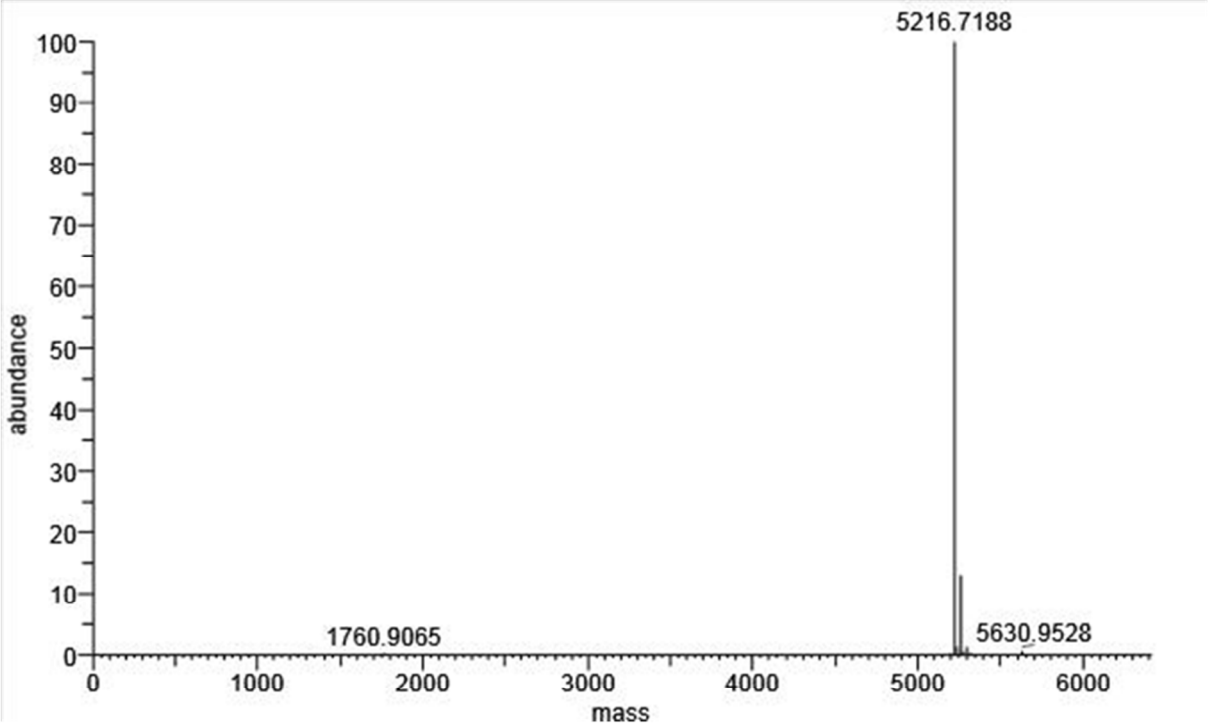

Xtract Mass Table				
Monoisotopic Mass	Sum Intensity	Number of Charge State	Average Charge	Delta Mass
5216.719	4109817	5	5.34	0
5259.721	542821	4	5.17	43.0021
5254.692	488033.6	5	5.8	37.9728
5238.749	68150.23	3	5.86	22.03
5296.686	58071.93	2	5.49	79.9676
5233.754	37278.56	2	6.41	17.0351
5276.707	33116.46	2	5.53	59.9879
5630.953	32377.3	2	5.51	414.234
5200.721	23522.44	1	5	-15.9976
5302.715	12985.98	1	5	85.9962
1760.907	10123.52	1	2	-3455.81
5315.678	9585.64	1	5	98.9596

Supplementary Figure 13: Deconvoluted mass spectrum of $M13_{M\text{-}5/28L}$ grown with 10 mM Aha/235 µM Met and reacted with 30 µM DBCO-PEG_4-biotin via the SPAAC reaction. This spectrum was obtained utilizing a Fisher Scientific ESI-orbitrap instrument.

Binding of dual-labeled M13 phages to SA-conjugated magnetic particles. Due to the bioorthogonal nature of azide chemistry, dual-labeling of M13 utilizing SPAAC alongside acylation of primary amines by NHS-esters was explored. $M13_{A9M}$ amplified with Aha ($M13_{A9M}$-

Aha) was reacted with DIBAC-biotin via SPAAC and acylation was concurrently carried out with NHS-sulfo-cy7, a dye molecule, to introduce a label that could be monitored. An affinity assay with SA magnetic particles was carried out to confirm dual-labeled functionality of M13 particles. It was expected that if M13 particles indeed had both biotin and sulfo-cy7 labels present on the same M13 particles, then the sulfo-cy7 absorbance signal would be expected to be separated out alongside the biotin label when incubated with an affinity probe to capture the ligand. Due to the tight-binding nature of biotin binding to SA, recovering bound M13 from the SA magnetic particles was not done. Instead, the presence of M13 on the particles was confirmed using immuno-detection with anti-pVIII antibodies.

The absorbance spectra of solutions of different M13 conjugates were read before and after incubation with SA magnetic particles. An unmodified $M13_{A9M}$-Aha control showed low non-specific binding to the SA magnetic particles (**Supplementary Figure 14a**). This was indicated by 97.6 % of the M13 absorbance remaining in the supernatant after incubation with SA magnetic particles. For $M13_{A9M}$-Aha labeled with DIBAC-biotin only, 9.4 % of the M13 absorbance remained in the supernatant (**Supplementary Figure 14b**). This indicated that binding of biotinylated M13 to the SA magnetic particles occurred as expected. The negative control of $M13_{A9M}$-Aha labeled with NHS-sulfo-cy7 only showed minimal binding to SA magnetic particles over 30 min incubation time (**Supplemental Figure 14c**). The percent of M13 signal remaining in the supernatant was 94.1% and the sulfo-cy7 signal at 750 nm remaining in solution was 92.4%. When $M13_{A9M}$-Aha reacted with DIBAC-biotin and NHS-sulfo-cy7 was incubated with SA magnetic particles for 30 min M13 binding to the particles along with a decrease in sulfo-cy7 signal was observed (**Supplementary Figure 14d**). The decrease in M13 signal was comparable to the decrease in sulfo-cy7 signal at 750 nm. The M13 absorbance remaining in solution was 13.7% of the initial absorbance and the sulfo-cy7 absorbance remaining in solution was 9.7% of the initial absorbance. These experiments were consistent with what would be expected for M13 successfully labeled with both biotin and sulfo-cy7 labels.

Further confirming this analysis, M13 could be detected on the particles themselves through an immuno-detection assay with anti-pVIII antibodies and HRP detection of TMB (**Supplementary Figure 15a**). The TMB chromogenic signal produced from the SA magnetic particles incubated first with dual-labeled A9M was greater than the background signal from just

the particles themselves incubated with the same antibodies (**Supplementary Figure 15b**). This further confirmed that the decrease in M13 absorbance from the supernatant was due to binding of M13 to the magnetic particles and serves as a way of confirming indeed that M13 was bound to the particles themselves.

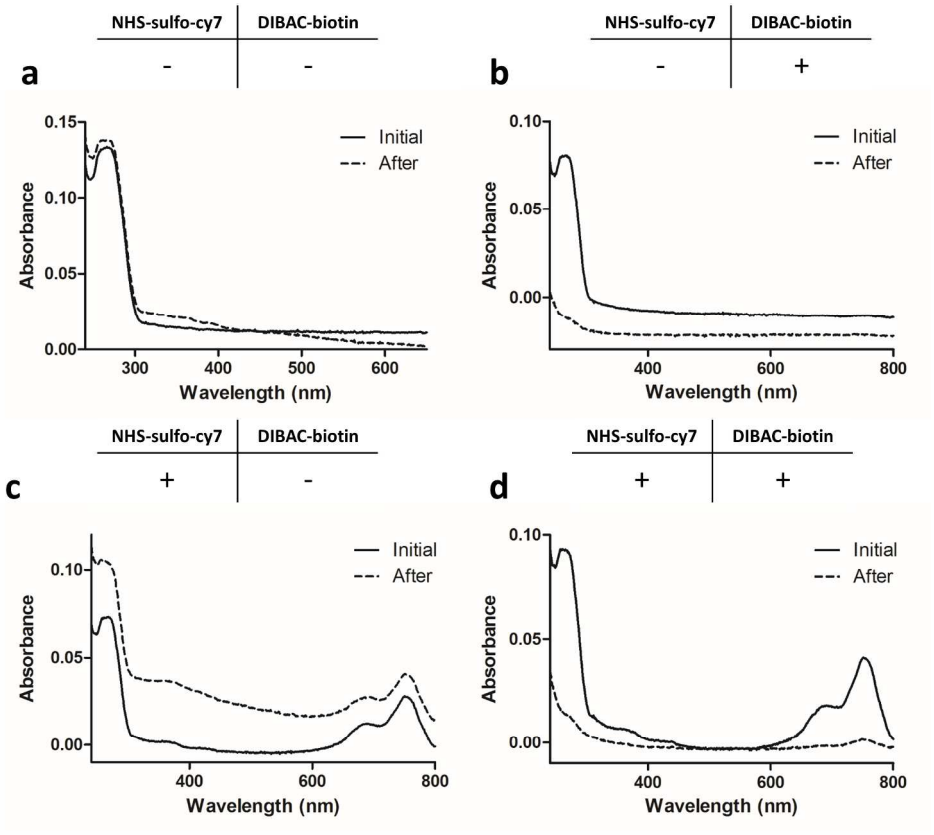

Figure 14: Comparison of the absorbance spectra of solutions of $M13_{A9M}$-Aha conjugates before and after separation with SA magnetic particles. The following conjugates of $M13_{A9M}$-Aha were prepared: (a) Unmodified $M13_{A9M}$-Aha only. (b) $M13_{A9M}$-Aha reacted with 30 µM DIBAC-TAMRA. (c) $M13_{A9M}$-Aha reacted with 100 µM NHS-sulfo-cy7. (d) $M13_{A9M}$-Aha reacted with 30 µM DIBAC-TAMRA and 100 µM NHS-sulfo-cy7. Then, 100 µL of each sample was incubated with 0.5 mg of SA magnetic particles for 30 min at 23 °C. SA magnetic particles were separated from the solution by applying a magnet for 2 min and the absorbance spectrum of the solution was read again.

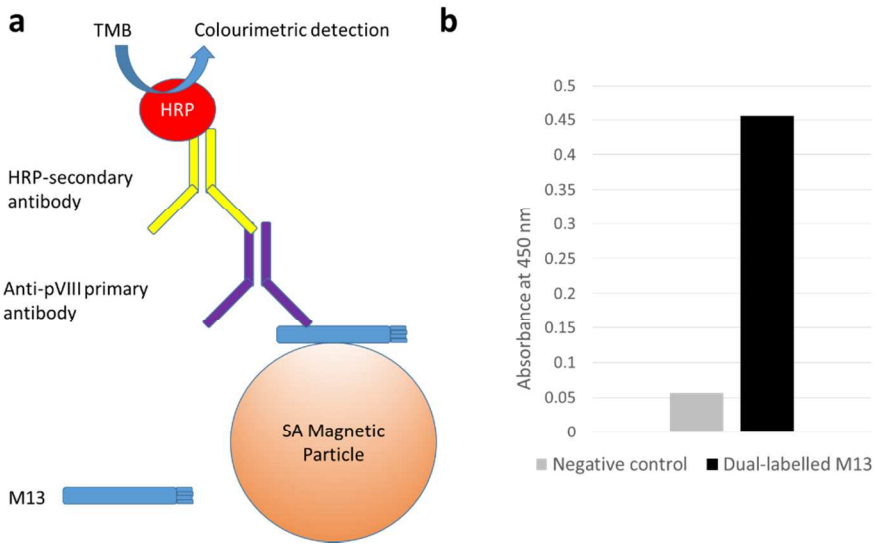

Figure 15: Immuno-detection of M13 bound to SA magnetic particles. (a) Schematic of immuno-detection protocol. The primary antibody used was anti-pVIII mouse IgG and the secondary antibody was goat anti-mouse IgG conjugated to HRP (b) Absorbance of TMB solution after immuno-detection and reaction with HRP. TMB solution was incubated with samples for 1.5 min and H_2SO_4 was added to a final concentration of 0.25 M to terminate the reaction.

References

(1) Wall, J. D., and Harriman, P. D. (1974) Phage P1 mutants with altered transducing abilities for Escherichia coli. *Virology 59*, 532–544.

(2) Baba, T., Ara, T., Hasegawa, M., Takai, Y., Okumura, Y., Baba, M., Datsenko, K. A., Tomita, M., Wanner, B. L., and Mori, H. (2006) Construction of Escherichia coli K-12 in-frame, single-gene knockout mutants: the Keio collection. *Mol. Syst. Biol. 2*, 2006.0008.

(3) Wezenbeek, P. M. van, Hulsebos, T. J., and Schoenmakers, J. G. (1980) Nucleotide sequence of the filamentous bacteriophage M13 DNA genome: comparison with phage fd. *Gene 11*, 129–148.

(4) Hest, J. C. van, Kiick, K. L., and Tirrell, D. A. (2000) Efficient incorporation of unsaturated methionine analogues into proteins in vivo. *J. Am. Chem. Soc. 122*, 1282–1288.

(5) Mourez, M., and Collier, R. J. (2004) Use of phage display and polyvalency to design inhibitors of protein-protein interactions. *Methods Mol. Biol. 261,* 213–227.

(6) Berkowitz, S. A., and Day, L. A. (1976) Mass, length, composition and structure of the filamentous bacterial virus fd. *J. Mol. Biol. 102*, 531–547.

(7) Meadows, D. L., Shafer, J. S., and Schultz, J. S. (1991) Determining the extent of labeling for tetramethylrhodamine protein conjugates. *J. Immunol. Methods 143*, 263–272.

(8) Ploss, M., and Kuhn, A. (2010) Kinetics of filamentous phage assembly. *Phys. Biol. 7*, 045002.

(9) Zhang, H., and Meyerhoff, M. E. (2006) Gold-coated magnetic particles for solid-phase immunoassays: enhancing immobilized antibody binding efficiency and analytical performance. *Anal. Chem. 78*, 609–616.

(10) Bos, E., Doelen, A. Van der, Rooy, N. van, and Schuurs, A. H. (1981) 3, 3', 5, 5'-Tetramethylbenzidine as an Ames test negative chromogen for horse-radish peroxidase in enzyme-immunoassay. *J. Immunoass. Immunoch. 2*, 187–204.

(11) Russel, M., and Model, P. (1989) Genetic analysis of the filamentous bacteriophage packaging signal and of the proteins that interact with it. *J. Virol. 63*, 3284–3295.
(12) Lubkowski, J., Hennecke, F., Plückthun, A., and Wlodawer, A. (1998) The structural basis of phage display elucidated by the crystal structure of the N-terminal domains of g3p. *Nat. Struct. Mol. Biol. 5*, 140–147.